recycling

MDPI

Article

Valorization of Minimally Processed Blast Furnace Slag in Industrial Mortars: Early-Age Performance and Embodied Carbon Reduction

Houssam Affan [1], Laurent Fehr [1], Ginan Al-Massri [2,*], Farjallah Alassaad [3], Amro Yaghi [3] and Hassan Ghanem [2,*]

[1] Groupe FEHR, Laboratoire Béton, 62 Route de Strasbourg, 67242 Bischwiller, France; houssam.affan@fehrgroup.com (H.A.); laurent.fehr@fehrgroup.com (L.F.)
[2] Faculty of Engineering, Beirut Arab University, Beirut 12-5020, Lebanon
[3] College of Engineering and Technology, American University of the Middle East, Egaila 54200, Kuwait; farjallah.alassaad@aum.edu.kw (F.A.); amro.yaghi@aum.edu.kw (A.Y.)
* Correspondence: g.massri@bau.edu.lb (G.A.-M.); h.ghanem@bau.edu.lb (H.G.)

Abstract

Conventional valorization of blast furnace slag commonly involves granulation, fine grinding, mechanical activation, or chemical activation, which increase energy demand and processing complexity. This study investigated a minimally processed blast furnace slag (MP-BFS), defined here as the fraction passing 64 μm obtained by sieving a 0–8 mm industrial material without grinding, additional granulation, thermal treatment, or chemical activation. MP-BFS replaced 10–50% of the cement by mass to reduce clinker in industrial mortars formulated at a constant flow spread of 23–24 cm and tested from 8 h to 90 d. Bulk density, water-accessible porosity, total and capillary water absorption, and compressive and flexural strengths were evaluated. Replacing 10% of the cement with slag improved compressive strength from the earliest test age and increased the 28-day compressive and flexural strengths by 5.1% and 9.5%, respectively, relative to the control mortar; this response coincided with a reduction in measured porosity from 8.95% to 8.01%. This improvement is consistent with a physical filling effect and improved particle packing, although these mechanisms were not directly verified by microstructural analyses. At higher replacement levels, water-accessible porosity increased, reaching 24.45% at 50% slag replacement, alongside greater water ingress and delayed strength development. Exploratory empirical regression analyses described associations among slag content, porosity, water transfer, and compressive strength within the investigated formulations. A simplified screening-level constituent-production-and-transport comparison per cubic meter, based on generic ICE factors and an assumed 50 km transport distance, estimated a maximum embodied carbon reduction of 44% at 50% replacement. Curing energy, use, carbonation, maintenance, and end-of-life stages were excluded. Overall, 10% MP-BFS replacement provided the most favorable performance–carbon content balance, whereas 30–50% achieved larger carbon reductions but showed early-age strength losses that limit their suitability for rapid-demolding applications under the investigated conditions.

Keywords: minimally processed blast furnace slag; industrial mortar; early-age strength; cement replacement; porosity; mechanical performance; embodied carbon

Check for updates

Academic Editor: Michele John

Received: 30 May 2026
Revised: 7 July 2026
Accepted: 10 July 2026
Published: 14 July 2026

Copyright: © 2026 by the authors. Licensee MDPI, Basel, Switzerland. This article is an open access article distributed under the terms and conditions of the Creative Commons Attribution (CC BY) license.

1. Introduction

The building industry is a major source of man-made carbon dioxide (CO_2) emissions. This is mostly due to the energy required for clinker production. Recent estimates show that cement production is responsible for about 7–8% of CO_2 emissions worldwide. Decarbonization of the building and public works sector is therefore a top concern [1,2]. In light of these environmental issues, research and industry are moving towards producing eco-friendly cementitious materials by replacing cement with mineral additives.

Reducing the clinker content of cementitious materials is widely recognized as one of the most technically accessible strategies for decreasing the embodied carbon of concrete and mortar [1,2]. Supplementary cementitious materials can contribute to this objective by partially replacing Portland cement while promoting the valorization of industrial by-products and industrial symbiosis between the steel and construction sectors. However, their environmental benefit depends not only on the cement replacement level but also on the processing route, transportation requirements, allocation assumptions, and functional performance of the resulting material [2]. The GCCA decarbonization roadmap accordingly identifies clinker factor reduction, increased use of supplementary cementitious materials, and circular utilization of industrial resources among the principal pathways toward net-zero concrete [3].

Blast furnace slag is one of the supplementary cementitious materials sourced from the steel industry. It is a by-product originating from the process of reducing iron ore and is mostly made up of calcium, silicon, aluminum, and magnesium oxides. When cooled and finely ground, slag shows latent hydraulicity, forming C–S–H-type hydration products in an alkaline environment [3,4]. Owing to its standardized composition, ground granulated blast furnace slag (GGBFS) has become a common ingredient in composite cements and high-durability concretes. Previous studies have shown that adding activated or crushed slag to cementitious materials enhances their properties, including durability, chemical resistance, lower hydration heat, and decreased permeability [5–15]. The reactivity of blast furnace slag can be enhanced through granulation, fine grinding, mechanical activation, or chemical and alkaline activation. Although these processing routes can improve slag dissolution and early-age performance, they introduce additional energy, material, cost, and operational requirements [15–18]. Alkali-activated materials constitute a distinct valorization route involving the use of alkaline activators and specific processing and handling conditions [3]. Therefore, the environmental advantage of direct or minimally processed slag utilization may arise not only from Portland cement substitution but also from avoiding some of the additional processing stages required for finely ground or activated slag systems. The magnitude of this benefit nevertheless depends on the system boundaries and assumptions adopted in the environmental assessment. In contrast to finely ground or activated slag, coarse or non-activated blast furnace slag generally exhibits lower early-age reactivity. The literature commonly attributes this behavior to a combination of lower specific surface area, limited dissolution kinetics, and, depending on the cooling history of the slag, a lower proportion of reactive amorphous phases [7,8,19–22]. The limited early-age dissolution of Ca-, Si-, and Al-bearing phases may delay the formation of C-S-H- and C-A-S-H-type hydration products, thereby slowing strength development. At high replacement levels, this delayed contribution may not compensate for the dilution of Portland cement, potentially resulting in higher water-accessible porosity and lower early-age mechanical performance.

However, the effects of slag incorporation on porosity are not uniform and depend on the slag processing route, particle size, amorphous content, replacement level, curing conditions, testing age, and porosity measurement method. At early and intermediate ages, high contents of coarse or low-reactivity slag may increase the fraction of open pores accessible to

water because cement dilution is not yet compensated by slag reaction [7,20,22]. In contrast, reductions in interconnected porosity have been reported at 28 days or later in systems containing more reactive, finely ground, activated, or combined supplementary cementitious materials [23,24]. Therefore, these reported trends are not necessarily contradictory, as they refer to different slag characteristics and stages of microstructural development.

In addition to their lower specific surface area, minimally processed slag particles generally exhibit a coarser particle-size distribution and a less optimized particle morphology than commercially ground granulated blast furnace slag (GGBFS) [23,24]. These characteristics reduce the available reactive surface and may limit the physical filling and particle packing effects that are commonly achieved with finely ground slag. Consequently, MP-BFS is expected to exhibit lower latent hydraulic reactivity and slower hydration kinetics than conventional GGBFS, particularly at early ages.

At low replacement levels, physical filling, improved particle packing, and possible heterogeneous nucleation may contribute to matrix refinement, even when the direct hydraulic contribution of the slag remains limited. With prolonged curing, continued reaction of reactive slag phases may also promote progressive densification of the cementitious matrix. Nevertheless, high replacement levels have frequently been associated with increased sorptivity and immersion water absorption, particularly when the early-age contribution of the slag is insufficient to compensate for clinker dilution [25–28]. These results should be interpreted cautiously because water-accessible porosity characterizes only the interconnected pores accessible to water and does not provide direct information on total porosity or pore size distribution.

Prior studies on blast furnace slag-blended cementitious matrices concentrated on activated slag and were conducted under idealized laboratory circumstances at medium and long curing ages (28 days and beyond). In contrast, industrial mortars are subjected to industrial limitations, such as the need for quick formwork removal, high production rates, or the need to reach a certain level of mechanical strength at an early age. Therefore, the literature values obtained for GGBFS or activated systems cannot be transferred directly to a minimally processed industrial fraction.

Direct incorporation of minimally processed blast furnace slag could reduce Portland cement and clinker consumption while minimizing the additional energy and operational requirements associated with fine grinding and activation [1,29]. This approach supports the circular valorization of a steel industry by-product; however, the limited early-age reactivity of MP-BFS may restrict the replacement levels compatible with rapid industrial production. At high replacement levels, the combined effects of cement dilution, limited early-age slag reaction, and increased water demand may adversely affect water-accessible porosity and mechanical performance. The previous literature shows limited knowledge about the effect of minimally processed slag on the mechanical and hygro-physical properties of mortars, especially in a real-world industrial setting. In this work, the term minimally processed blast furnace slag (MP-BFS) refers specifically to the fraction obtained solely by sieving the supplied 0–8 mm material to below 64 µm, without grinding, additional granulation, thermal activation, or chemical activation. The principal novelty is the combined evaluation of this screened industrial fraction at replacement levels of 10–50% under a constant-flow formulation constraint, with measurements from 8 h to 90 d and a simplified embodied carbon comparison.

The objective of the present study is therefore not to compete directly with commercially produced ground granulated blast furnace slag (GGBFS), whose performance benefits from dedicated grinding and standardized processing. Instead, this work investigates whether a minimally processed industrial fraction can provide an acceptable balance between mechanical performance and embodied carbon reduction while avoiding addi-

tional energy-intensive processing. Consequently, the study evaluates a distinct industrial valorization pathway, recognizing that its performance limitations, particularly at early ages, may differ from those reported for conventional GGBFS systems.

Accordingly, this study evaluates the influence of minimally processed blast furnace slag (MP-BFS) content on early- and later-age mechanical performance, water-accessible open porosity, bulk density, and water uptake in industrial mortars formulated to a flow spread of 23–24 cm. Empirical regression analyses are used to describe associations among replacement level, porosity, capillary uptake, and compressive strength. The environmental comparison quantifies the effect of cement substitution under explicitly stated assumptions. Industrial production in the investigated plant is organized in three consecutive 8 h shifts. Consequently, the 8 h testing age corresponds to the intended demolding time at the end of one production shift, whereas the 24 h testing age corresponds to the subsequent handling and lifting stage. Under the investigated production conditions, the plant-specific operational requirement is a minimum compressive strength of 8 MPa at 8 h for demolding and 12 MPa at 24 h before handling. The latter requirement remains conditional on the design and verification of the lifting system, including the element geometry and self-weight, the position and embedment depth of the lifting anchors or inserts, the edge distances, the lifting configuration, and the associated dynamic effects [30,31]. These values are used as production-specific formulation-screening criteria and should not be interpreted as universal requirements applicable to all precast products.

2. Results and Discussion

2.1. Water-Accessible Open Porosity

Figure 1 presents the results of water-accessible open porosity for the mortars with different slag replacement levels. As shown, the reference mortar F0 exhibits an open porosity of 8.95%; this value decreases by 11% to reach 8.01% for F10, and then increases by 10.4%, 51.1%, 65.4%, and 173.2% for F20, F30, F40, and F50, respectively. These results indicate that the most significant increase in porosity occurs beyond a slag replacement level of 20%, with a pronounced jump between F20 and F30. This finding is consistent with data recorded in the existing literature regarding the use of low- or non-activated slag in cement matrices presented in Table 1. Previous studies have associated the limited early-age contribution of non-activated slag with slower matrix development and a more open water-accessible pore network [4,6,21,32]. Because the mixtures were formulated at constant flow, the increasing water-to-powder ratio may also have contributed to the higher porosity at elevated replacement levels. Moreover, porosity was measured only at 28 d; therefore, no direct conclusion regarding early-age pore structure evolution can be drawn. Moreover, the diluting effect of cement, combined with partial substitution by a slow-reacting additive, leads to a rise in the proportion of interconnected pores [33]. However, particle packing, hydration products, pore size distribution, and connectivity were not directly measured, so these mechanisms remain hypotheses rather than direct observations.

Table 1. Porosity of mortar incorporating low or non-activated slag.

Reference	Studied Matrix	Slag Replacement Level (%)	Water-Accessible Open Porosity (%)
B. Edeb et al. (2024) [34]	Mortars with slag	≤25	≈10%
Maléki Tagba et al. (2021) [35]	Mortars with slag, silica fume, and aggregates (natural and rubber)	20	≈15–20%
Ikhaddalene et al. (2025) [36]	Mortar with slag	10	≈19%

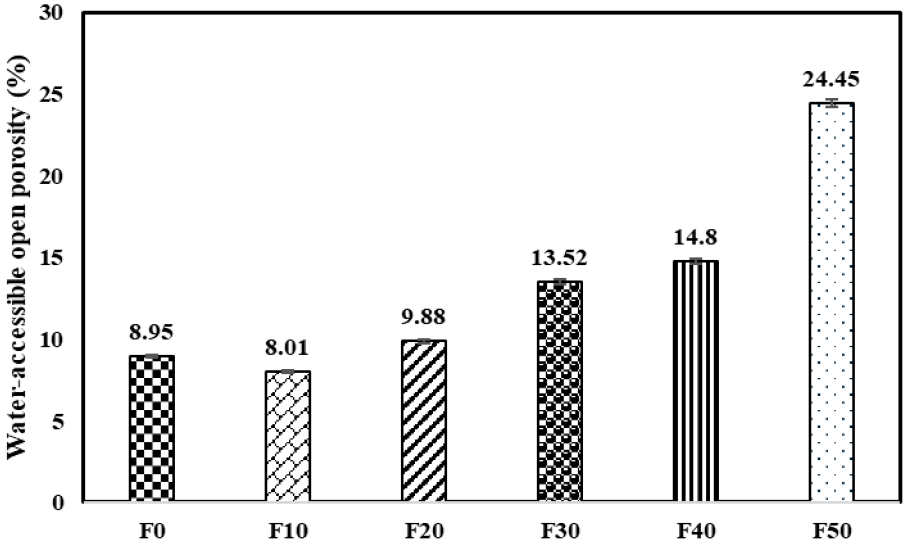


Figure 1. Variation in water-accessible open porosity of mortar mixtures with increasing slag replacement level.

These literature values are provided for qualitative comparison only because the binder systems, curing conditions, and measurement procedures differ among the studies.

2.2. Bulk Density

Bulk density results for various mortar mixes are illustrated in Figure 2. The results indicate that the apparent density gradually decreases as the amount of slag increases. The progressive decrease in bulk density is consistent with the increase in water-accessible open porosity observed at higher MP-BFS replacement levels [35,37]. The increasing mixing water demand may also have contributed to the lower hardened density by increasing the volume of water-accessible voids after drying.

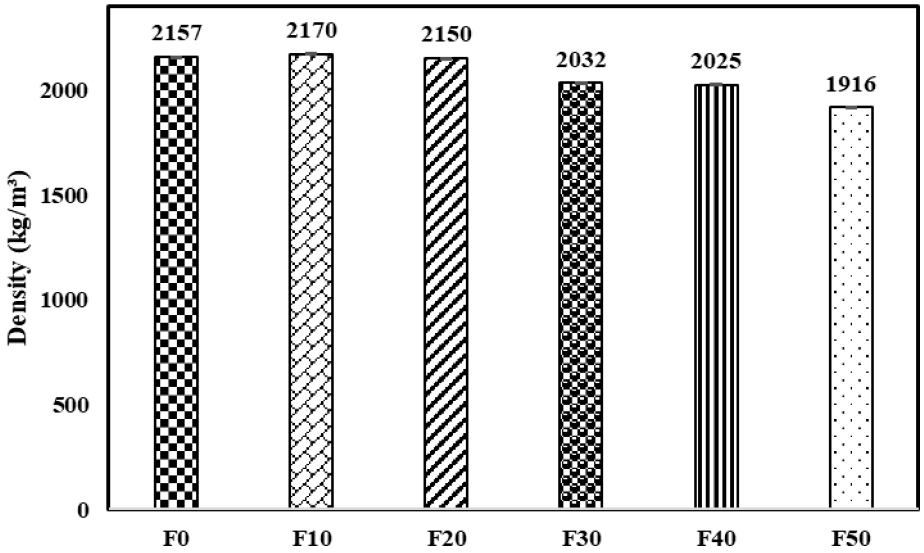


Figure 2. Variation in the bulk density of mortar mixtures as a function of slag replacement level.

Differences in constituent density, hydration development, and particle packing may additionally influence bulk density. However, the density and morphology of the incorporated MP-BFS fraction, the packing density, and the degree of hydration were not determined experimentally. These factors are therefore considered possible contributing mechanisms rather than directly demonstrated causes.

2.3. Water Absorption by Immersion

Table 2 shows the total water absorption values for all formulations at 28 d. The results reveal that the water absorption of the control mix F0 is 4.15% and then decreases to 3.69% for F10. Beyond 10%, total water absorption gradually increases with increasing slag replacement level to attain 12.76% for F50. Numerous studies indicate that water absorption through immersion depends on the volume and connectivity of open pores, especially continuous capillary pores [38]. The reduction in water absorption from 4.15% for F0 to 3.69% for F10 is consistent with the lower water-accessible open porosity measured for F10. This behavior may be associated with favorable filler or particle packing effects at low MP-BFS content, although these mechanisms were not directly investigated.

Table 2. Water absorption of mortar mixes with different slag replacement levels.

Formulation	Average Dry Weight (g)	Mass After 48 h Immersion in Water (g)	Absorption (%)
F0	552.2 ± 24.85	575.1 ± 20.12	4.15 ± 0.165
F10	555.4 ± 22.25	575.9 ± 20.15	3.69 ± 0.145
F20	550.5 ± 19.45	575.8 ± 23.03	4.59 ± 0.161
F30	520.2 ± 20.28	554.8 ± 22.75	6.65 ± 0.266
F40	518.5 ± 18.18	556.4 ± 22.25	7.31 ± 0.307
F50	490.4 ± 17.15	553.0 ± 16.55	12.76 ± 0.446

Beyond 10% replacement, water absorption increased progressively and reached 12.76% for F50. This increase cannot be attributed solely to MP-BFS incorporation because the mixtures were formulated at constant flow spread, and the mixing water content increased with the replacement level. The observed behavior may therefore result from the combined effects of higher water demand, Portland cement dilution, limited early-age contribution of MP-BFS, and changes in the water-accessible pore network [6,7].

2.4. Capillary Absorption Uptake

Figure 3 displays the mass of water absorbed by capillary water uptake as a function of the square root of time for the mortar mixes with varying slag replacement levels at 28 days. The results indicate the same trend, with capillary absorption increasing with time for all mixtures. At longer times, the rate of water uptake becomes less pronounced, and the curves tend toward a quasi-stabilized regime, suggesting a progressive refinement of the capillary network. When comparing the mixes, mortar with replacement levels beyond 30% presents steeper initial slopes and higher absorbed masses. This trend can be attributed to the increase in water-accessible porosity observed for the same mixtures. Similar increases in capillary absorption and sorptivity have been reported for mortars incorporating blast furnace slag [6,7].

The interpretation of the mortar behavior is based on mechanical performance, water-accessible open porosity, water absorption, and capillary water absorption measurements. No direct microstructural characterization was performed using XRD, SEM/EDS, TGA/DTG, MIP, or related techniques. Consequently, explanations involving delayed MP-BFS reaction, hydration product formation, particle packing effects, and refinement of the water-accessible pore network are considered literature-supported interpretations consistent with the experimental trends rather than mechanisms directly verified in the present study.

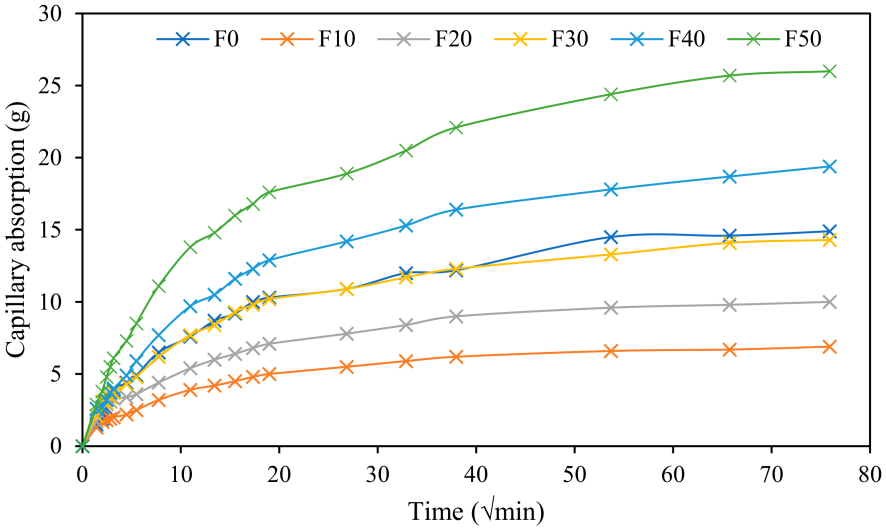


Figure 3. Capillary absorption of mortar mixes with different slag replacement levels.

2.5. Compressive Strength

Figure 4 shows the compressive strength of mortars made with MP-BFS for replacement ratios of 0%, 10%, 20%, 30%, 40%, and 50% (F0–F50) at ages of 8 h, 1 d, 7 d, 28 d, and 90 d. Although compressive strength increases with age for all mixes, the level of strength and gain rates are clearly affected by slag replacement ratios.

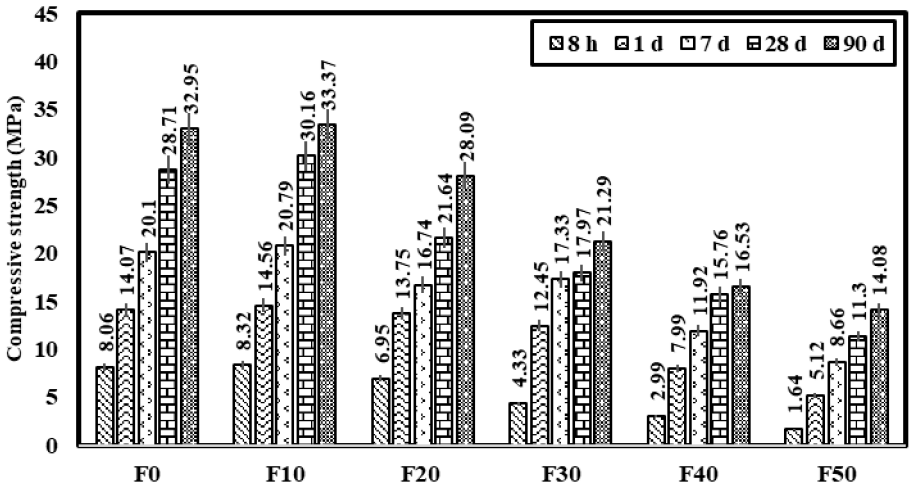


Figure 4. Compressive strength of mortar mixes with different slag replacement levels.

The reference mix F0 shows a continuous increase in compressive strength from 8.06 MPa at 8 h to 14.07 MPa at 1 d, 20.10 MPa at 7 d, 28.71 MPa at 28 d, and 32.95 MPa at 90 d. The gain rates between consecutive ages are +42.6% (8 h→1 d), +43.0% (1 d→7 d), +42.8% (7 d→28 d), and only +14.8% (28 d→90 d), suggesting that compressive strength development is dominated by cement hydration up to 28 days and strength gain at later ages is much slower. Compressive strength development of F10 follows the same trend: At 8 h and 1 d, F10 reached compressive strengths of 8.32 and 14.56 MPa, respectively, exceeding the corresponding values of the control mix. Although at late age, the strength gain is reduced again, the strength still remains much higher than the reference mix, reaching ~105% of the reference strength at 28 d and remaining above that level at 90 d.

The simultaneous improvement in compressive strength and reduction in water-accessible open porosity observed for F10 are consistent with possible physical filler, particle packing, or heterogeneous nucleation effects at low MP-BFS content. However, the relative

contributions of these physical mechanisms and any chemical contribution of MP-BFS cannot be distinguished without direct microstructural and hydration measurements.

For slag replacement levels beyond 20%, early-age compressive strength shows deterioration. At 8 h, it drops by 13.8%, 46.3%, 62.9%, and 79.6% relative to F0 for F20, F30, F40, and F50, respectively. This trend remains at 1 and 7 days, reflecting a pronounced delay in strength development. At 28 days, F20, F30, F40, and F50 reach 75%, 62.6%, 54.9%, and 39.4% of the reference strength. The strength reductions at high replacement levels also reflect the progressively increasing water demand and cannot be attributed exclusively to MP-BFS replacement. The parent 0–8 mm slag contained a total Zn concentration of 6310 mg/kg. Zinc-bearing species are known to retard Portland cement hydration, particularly through inhibition of C_3S dissolution and the formation or adsorption of Zn-containing phases on unhydrated cement surfaces. Therefore, a Zn-related chemical-retardation effect may have contributed to the early-age strength reductions observed at high MP-BFS contents [4]. However, its contribution cannot be quantified from the present results because Zn was measured in the parent 0–8 mm material rather than specifically in the fraction passing 64 μm, while Zn speciation, aqueous availability, hydration heat, and hydration product evolution were not determined. The observed performance losses are therefore interpreted as the combined outcome of cement dilution, increasing water demand, limited early-age MP-BFS contribution, changes in particle packing, and possible trace element-related retardation.

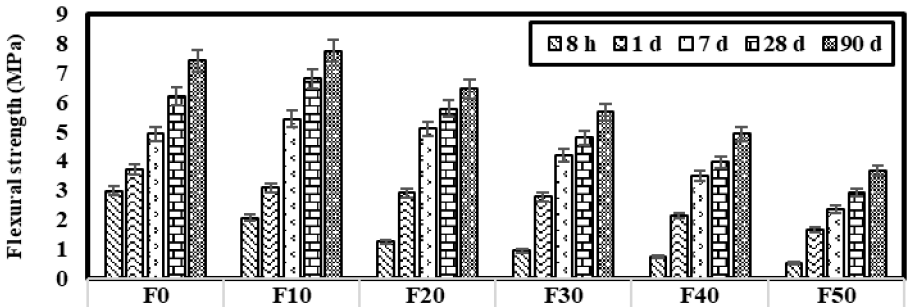
From an industrial perspective, the 8 h results were compared with the plant-specific demolding requirement of 8 MPa. F0 and F10 reached 8.06 and 8.32 MPa, respectively, and therefore satisfied the demolding criterion. In contrast, F20, F30, F40, and F50 reached 6.95, 4.33, 2.99, and 1.64 MPa, respectively, and did not satisfy the 8 h requirement. At 24 h, F0 and F10 reached 14.07 and 14.56 MPa, respectively, thereby exceeding the plant-specific handling criterion of 12 MPa. Nevertheless, compliance with the compressive-strength criterion does not replace the verification of the lifting anchors and the handling configuration for the actual precast element.

The continued strength gain between 28 and 90 d is consistent with a possible delayed contribution of MP-BFS together with continued cement hydration; however, these contributions cannot be separated without direct hydration or microstructural measurements. Whereas, at higher slag replacement levels, the late-age strength gain does not compensate for the early strength loss. At 90 days, compressive strengths of 28.09 MPa (F20), 21.29 MPa (F30), 16.53 MPa (F40), and 14.08 MPa (F50) are recorded, which remain 14.8%, 35.4%, 49.8%, and 57.3% lower than the control mixture, respectively. Taken together, these results show that a low slag substitution level (10%) preserves and may even slightly enhance compressive strength over the entire curing period, whereas higher replacement levels lead to persistent strength losses that are particularly critical at early ages, despite continued strength development at later times.

Such a strength evolution, combining stable performance at low slag contents with pronounced early-age penalties at higher replacement levels, agrees well with previous studies reporting delayed hydration and strength development in mortars containing MP-BFS [6,20,39,40].

2.6. Flexural Strength

The flexural strength results of mortars incorporating MP-BFS at replacement levels of 0%, 10%, 20%, 30%, 40%, and 50% (F0–F50) and tested at curing ages of 8 h, 1 d, 7 d, 28 d, and 90 d are presented in Figure 5. The results indicate that flexural strength increases with curing age for all mixtures, whereas increasing slag replacement generally leads to a reduction in strength, particularly at early ages.



	F0	F10	F20	F30	F40	F50
8 h	2.98	2.06	1.25	0.93	0.72	0.51
1 d	3.71	3.08	2.9	2.77	2.13	1.66
7 d	4.92	5.43	5.09	4.19	3.48	2.35
28 d	6.2	6.79	5.77	4.79	3.96	2.92
90 d	7.41	7.75	6.44	5.66	4.91	3.66

Figure 5. Variation in flexural strength of mortar mixtures as a function of slag replacement level.

A comparable trend was observed at 8 h and 1 d: F0 exhibits the highest flexural strength, while the incorporation of slag sharply decreases the strength to reach 0.51 MPa at 8 h and 1.66 MPa at 1 d for F50. At 8 h, the flexural strength of F0 is 2.98 MPa.

At 7 d, the flexural strength further increases, with F0 attaining 4.92 MPa. The 10% replacement level increases the reference strength by 10.4% to reach 5.43 MPa, while the 20% replacement level shows a strength close to that of the control at 5.09 MPa (+3.5%). When the slag content varies between 30% and 50%, the flexural strength drops by 14.8–52.2%, respectively.

At 28 d, F10 exhibits a flexural strength higher than the reference strength by 9.5%, while 20% cement replacement reduces the strength by 6.9%. This suggests that flexural performance was less sensitive than compressive performance to moderate MP-BFS replacement under the investigated conditions. Flexural strength loss is more noticeable for higher replacement levels, reaching 52.9% of the control strength for F50.

A similar pattern is observed at 90 d. F10 remains the best-performing mix, outperforming the control mix by 4.6%, while F20 shows a strength decrease of 13.1%. For higher replacement levels, late-age gains are observed, with values of 5.66 MPa (F30; −23.6%), 4.91 MPa (F40; −33.7%), and 3.66 MPa (F50; −50.6%). The strength increase between 28 and 90 d is particularly evident for these mixtures, indicating continued strength development that may include a delayed contribution of MP-BFS together with continued cement hydration. However, this interpretation remains tentative because particle packing, fracture behavior, interfacial characteristics, and microstructure were not directly investigated.

3. Exploratory Empirical Relationship Analysis

3.1. Objective and General Approach

Along with experimental testing, empirical modelling was suggested to meet three goals: (i) to understand the effect of minimally processed slag on hygro-physical and mechanical properties, (ii) to check the accuracy of measurements using known laws, and (iii) to predict relationships between parameters in order to enhance the performance of the mixes. The chosen method connects the mix proportions to the porous network, which directly affects water transport and mechanical strength. This connection fits well with the "formulation → microstructure → properties" framework that is commonly used for cementitious materials. The principle of establishing a relationship between the replacement rate and a given property, or between two properties, is well documented in the scientific literature [41–45]. Numerous studies have shown that modifying the replacement rate of cement with mineral additives (such as limestone fillers, fly ash, or

slag) directly influences the porosity of the mortar, which is in turn strongly correlated with its mechanical and physical properties. For example, Benachour et al. demonstrated a linear increase in mortar porosity with increasing limestone filler replacement level, accompanied by a progressive deterioration of the mechanical performance [45]. Similarly, Li et al. showed the existence of an optimal replacement rate of mineral additives at which the mechanical properties are optimized by reaching a minimum porosity of cement paste and mortar [44]. Moreover, Papayianni and Stefanidou demonstrated a robust inverse relationship between the porosity and the compressive strength of mortars, regardless of the binder [41].

3.2. Porosity Modeling: From Formulation to Porous Network

The hygric properties of the cementitious materials are controlled by the water-accessible porosity, which is strongly related to the mixture and the clinker replacement level. In this investigation, an empirical model was developed to connect the slag replacement level to the water-accessible porosity of the mortars, with the goal of assessing the effect of the MP-BFS on the porous network. A second-order polynomial regression was used to describe the relationship between MP-BFS replacement level and water-accessible open porosity, which is expressed as:

$$\phi(r) = ar^2 - br + c \quad (1)$$

where:

$\varnothing(r)$ = Water-accessible porosity

r = Slag to binder ratio (0, 0.1, 0.2, 0.3, 0.4, and 0.5)

a, b, c = Regression coefficients

Figure 6 shows both measured and predicted water-accessible porosity. The high coefficient of determination (R^2 = 0.96) indicates good agreement between the fitted values and experimental findings and shows that the proposed model reliably captures the evolution of porosity with slag replacement level.

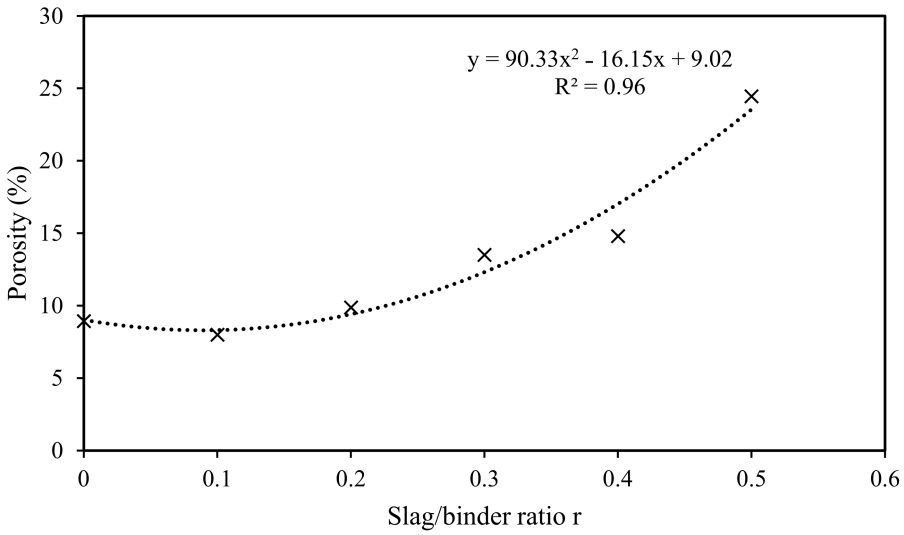


Figure 6. Comparison between measured and fitted water-accessible porosity of mortar mixtures containing different slag replacement levels.

The experimental and empirical results indicate that water-accessible porosity increases in a distinctly non-linear manner as the proportion of MP-BFS rises. At low substitution levels (F10–F20), porosity remains close to that of the reference mortar, suggesting that the clinker dilution effect is partially offset by improved particle packing and a filler

contribution from the fine slag fraction. Comparable behavior has been reported in the literature for cementitious systems incorporating low- or moderately reactive mineral additions, where limited replacement does not significantly disrupt the pore structure [38,46].

For slag replacement levels exceeding 30%, the evolution of porosity changes noticeably. At higher substitution rates, the reduction in clinker content becomes the dominant factor, while the contribution of MP-BFS to early hydration remains limited. As a result, the amount of hydration products formed at early ages is insufficient to efficiently occupy the capillary space, which leads to a more open and increasingly interconnected pore structure. Comparable observations have been reported for low-clinker binders and cementitious systems incorporating mineral additions with delayed reactivity [47,48].

The close agreement between modeled and experimental porosity trends further suggests that slag content plays a dominant role in governing the development and refinement of the porous structure in the investigated mortars. In addition, the relatively small dispersion of the data around the fitted curve suggests that the influence of slag on porosity is stable and reproducible under the current curing conditions. This result highlights formulation as an effective means of adjusting microstructural porosity and, consequently, the performance of mortars incorporating industrial by-products.

3.3. Sorptivity Modeling: From Porous Network to Water Transfer

Water ingress into cementitious materials depends on many factors: porosity, capillary pore size, and pore connectivity. Based on the classic capillary flow theory (Washburn's law), capillary absorption in cementitious materials is commonly described using a square-root-of-time relationship:

$$\Delta m(t) = s\sqrt{t} \quad (2)$$

where:

Δm = Quantity of absorbed water (g)

S = Sorptivity (g/$\sqrt{}$min)

T = Time (min)

Figure 7 demonstrates that the fitted relationship describes the experimental trend for all slag replacement levels. This validation is reflected by high coefficients of determination ranging from 0.77 to 0.97 for all mixes.

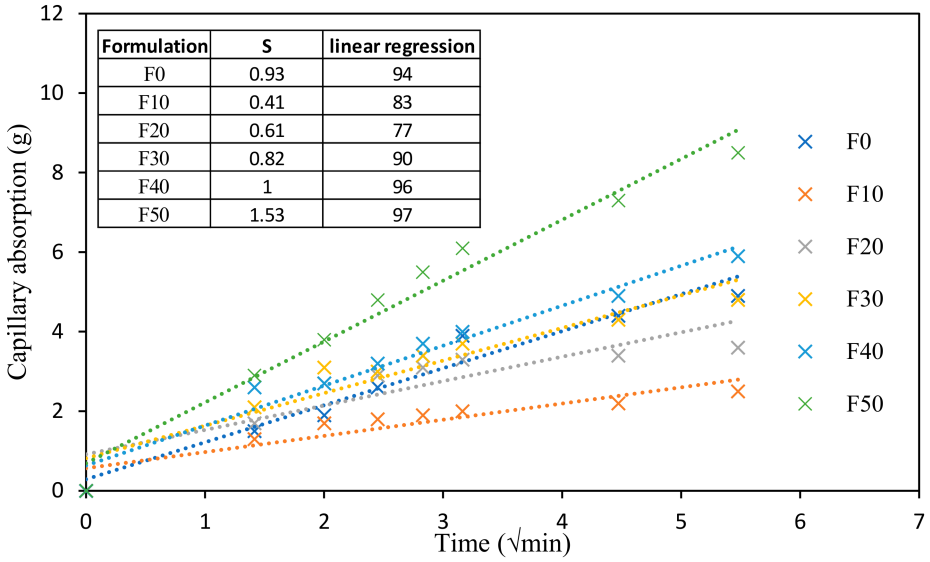


Figure 7. Empirical agreement with the experimental data of capillary absorption.

Initially, all formulations exhibited a linear relationship, validating that water transfer is primarily governed by capillarity. The sorptivity, representing the slope of the regression lines, increases with porosity. This trend shows that when the water-accessible porosity increases, the capillary network becomes more connected, which promotes water movement by suction. For low replacement levels (F10 and F20), sorptivity coefficients remain low, which may be attributed to their porosity being comparable to that of the control. Contrarily, for replacement levels of 40% and 50%, sorptivity increases notably, signifying a more open and interconnected porous network. This phenomenon corresponds with microstructural models of cementitious pastes and mortars, indicating that an increase in capillary porosity and a decrease in the amount of hydration products facilitate accelerated water transfer [38,41,48]. Similar patterns have been observed in matrices integrating mineral additives with reduced or delayed reactivity [46,47]. The link between porosity, sorptivity, and immersion absorption shows that the porous network is the main microstructural factor that controls water ingress through the matrix. Adding MP-BFS mostly affects this porous network by slowly increasing the network's ability to absorb and move water. In this context, the "porosity → water transfer" model confirms the experimental measurements and supports a direct relationship between MP-BFS and the water movement.

3.4. Strength Modeling: From Porous Network to Mechanical Performance

The mechanical properties of cementitious materials are highly controlled by their microstructure, especially their porous network. An exponential model of the Ryshkevich type was chosen to measure this relationship. This approach was originally suggested for porous materials; nevertheless, it has been extended for cementitious materials to correlate mechanical strength with porosity [48]. The overall relationship is as follows:

$$CS = CS_0 e^{(-k\phi)} \quad (3)$$

where:

CS = Compressive strength (MPa)

CS_0 = Extrapolated strength for zero porosity (MPa)

ϕ = Water-accessible porosity (volume percent vol.%)

k = Fitting coefficient relating strength to porosity

This model is suitable for cementitious materials with non-uniform porous networks because it takes into account the non-linearity between the strength loss and the porosity. Based on the experimental results of compressive strength and porosity evaluated at 28 d for formulations F0 to F50, CS0 and k were determined.

Figure 8 shows the relationship between the 28-day compressive strength and the water-accessible porosity. The experimental data points are compared to the fit of the exponential model, showing a decrease in compressive strength as porosity increases. The coefficient of determination (R^2 = 0.88) shows that the model and the experimental data agree well, although cementitious materials are naturally variable.

The results are consistent with the observed relationship that water-accessible porosity is the main microstructural factor that affects the compressive strength. Formulations with low porosity, namely F0 and F10, exhibited water-accessible porosity values of 8.95% and 8.01%, respectively, and developed the highest compressive strengths at 28 days (28.71 MPa and 30.16 MPa) and 90 days (32.95 MPa and 33.37 MPa). In contrast, increasing slag replacement led to a progressive rise in porosity, reaching 24.45% for F50, which corresponded to a marked reduction in compressive strength to 11.30 MPa at 28 days and 14.08 MPa at 90 days. This represents a strength loss of approximately 62% at 28 days compared to F10, confirming the strong inverse relationship between porosity and mechanical performance. This phenomenon corresponds with the recognized microstructural models of cementitious

materials, which assert that an increase in capillary pore volume simultaneously results in a decrease in the continuous solid fraction that can support mechanical loads [38,49,50]. Moreover, a more open porosity network has been demonstrated to facilitate the onset and propagation of cracks under load, consequently leading to a reduction in compressive strength. When mortars incorporate MP-BFS, this change is even more noticeable due to the slag's delayed reactivity. At 28 d, the hydration products are insufficient to compensate for the clinker dilution effect, rendering the material more porous and therefore weaker. A comparable series of observations has been documented in the literature regarding materials that include mineral additives exhibiting delayed reactivity [47,51]. The proven association between porosity and mechanical strength offers a mechanistic explanation for the impact of MP-BFS on mortar performance. The results indicate that the reduction in mechanical strength observed at higher substitution rates is primarily governed by the increase in porosity. On this basis, the proposed model provides an empirical description of strength evolution and a quantitative framework for guiding mix design optimization.

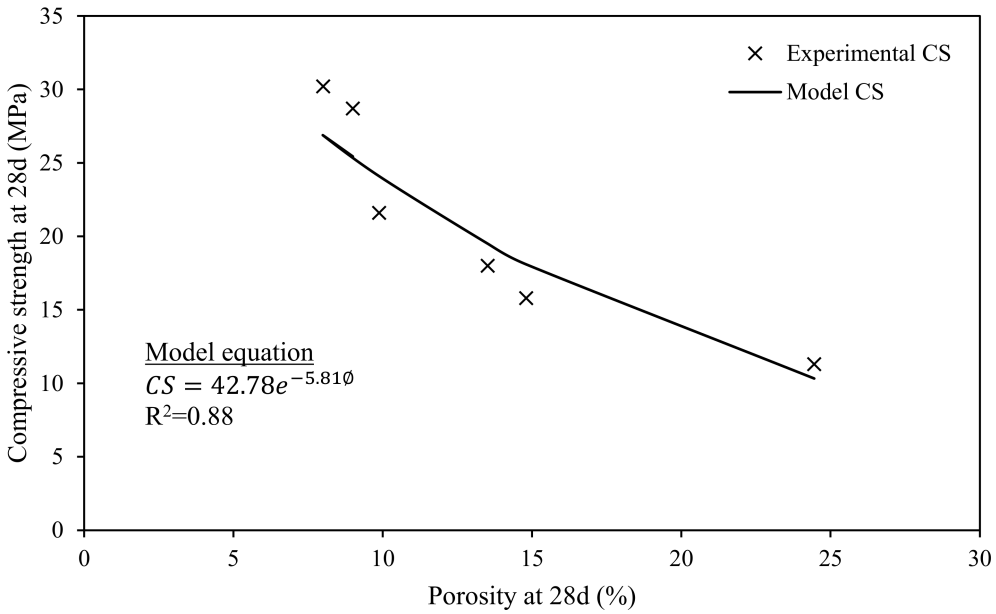


Figure 8. Experimental and modeled compressive strength versus water-accessible porosity at 28 days.

The model should consequently be regarded as an empirical formulation-specific relationship rather than a validated general predictive law. The fitted equation is applicable only within the investigated MP-BFS replacement range (0–50%) and should not be extrapolated beyond the studied formulations, materials, or curing conditions without additional validation. Additional mixtures and independent validation data would be required before applying the fitted parameters outside the investigated system.

4. Simplified Embodied Carbon Assessment

A simplified embodied carbon assessment was conducted to compare the mortar formulations. The functional unit was defined as 1 m^3 of fresh mortar. The system boundary included the production of the constituent materials and their assumed transport to the mortar production facility. The embodied carbon of each formulation was calculated as:

$$EC_{m^3} = \sum_i (m_i \times EF_i) + EC_{\text{transport}} + EC_{process} + EC_{\text{Losses}} \quad (4)$$

where m_i is the mass of the constituent i (kg/m^3) and EF_i is its emission factor (kg CO_2e/kg), supplemented by contributions from the ICE model for transport, process, and loss. $EC_{\text{transport}} + EC_{process} + EC_{\text{Losses}}$ represent the transport, processing, and material loss contributions (on mortar mixing), respectively, calculated according to the assumptions and factors provided in the Inventory of Carbon and Energy database [52].

The boundary covers the comparative production and assumed transport of constituents. It excludes the energy required for the <64 µm sieving operation, energy for the 40 °C conditioning stage, allocation or avoided burden scenarios for the slag, carbonation uptake, use and maintenance, and end-of-life. The assessment is therefore considered a simplified screening-level embodied carbon assessment rather than a complete ISO 14040 [53].compliant life-cycle assessment (LCA). It is used only for relative comparison among formulations under the defined assumptions and system boundaries. These emission factors used for each raw material were obtained from the ICE database [52]. Regarding slag, this database provides a value of 0.0416 kgCO_2/kg for treated granulated slag [52]. However, the absence of granulation and fine grinding in this investigation significantly reduces the energy consumption, as discussed in some studies [54–57]. The corresponding reduction in processing emissions could not be quantified because plant-specific energy data for sieving and material handling were unavailable. No additional avoided burden credit or alternative mass- or economic-allocation scenario was applied to the slag. Consequently, the reported values depend on the selected ICE proxy and should be interpreted as comparative estimates rather than material-specific life-cycle results. The use of the granulated slag factor may overestimate the production impact of MP-BFS, but the magnitude of this potential overestimation cannot be determined from the available data. A formal sensitivity analysis was not conducted because no independent and sufficiently documented alternative emission factors were available for the investigated MP-BFS. Introducing arbitrary lower factors would have increased the numerical variability without improving the reliability of the assessment. A transport distance of 50 km from the source of each constituent to the mortar production facility was assumed for the comparative calculation [1,16,57,58].

The carbon impact results are presented in Figure 9a,b. The findings show a decrease in greenhouse gas emissions with the substitution rate of MP-BFS. The estimated cement contribution decreases sharply with substitution: 313.4, 282.2, 251.0, 219.1, 187.9, and 156.7 kg CO_2e·m^{-3} for F0, F10, F20, F30, F40, and F50, respectively. Non-binder contributions, defined as the difference between total embodied carbon and the binder contribution, remain relatively stable at around 25–32 kg CO_2e·m^{-3}, which highlights the significant impact of variations in cement on embodied carbon.

Taking the whole composition into consideration, the reference mortar F0 has an impact of 339 kgCO_2e/m^3. As shown in Figure 9a, greenhouse gas emissions are 309, 279, 248, 218, and 189 kgCO_2e/m^3 for 10%, 20%, 30%, 40%, and 50%, respectively. As illustrated in Figure 9b, these reductions correspond to embodied carbon savings of approximately 9%, 18%, 27%, 35%, and 44% compared to the reference mix. Under the adopted ICE factors and system boundary, the estimated embodied carbon decreased nearly linearly with increasing MP-BFS replacement. This trend primarily reflects the reduction in Portland cement content, which represents the dominant contribution to the calculated impact. The estimated reductions of 9–44% are consistent with values reported for cementitious materials containing substantial proportions of low-activity slag [24,55,56,59,60].

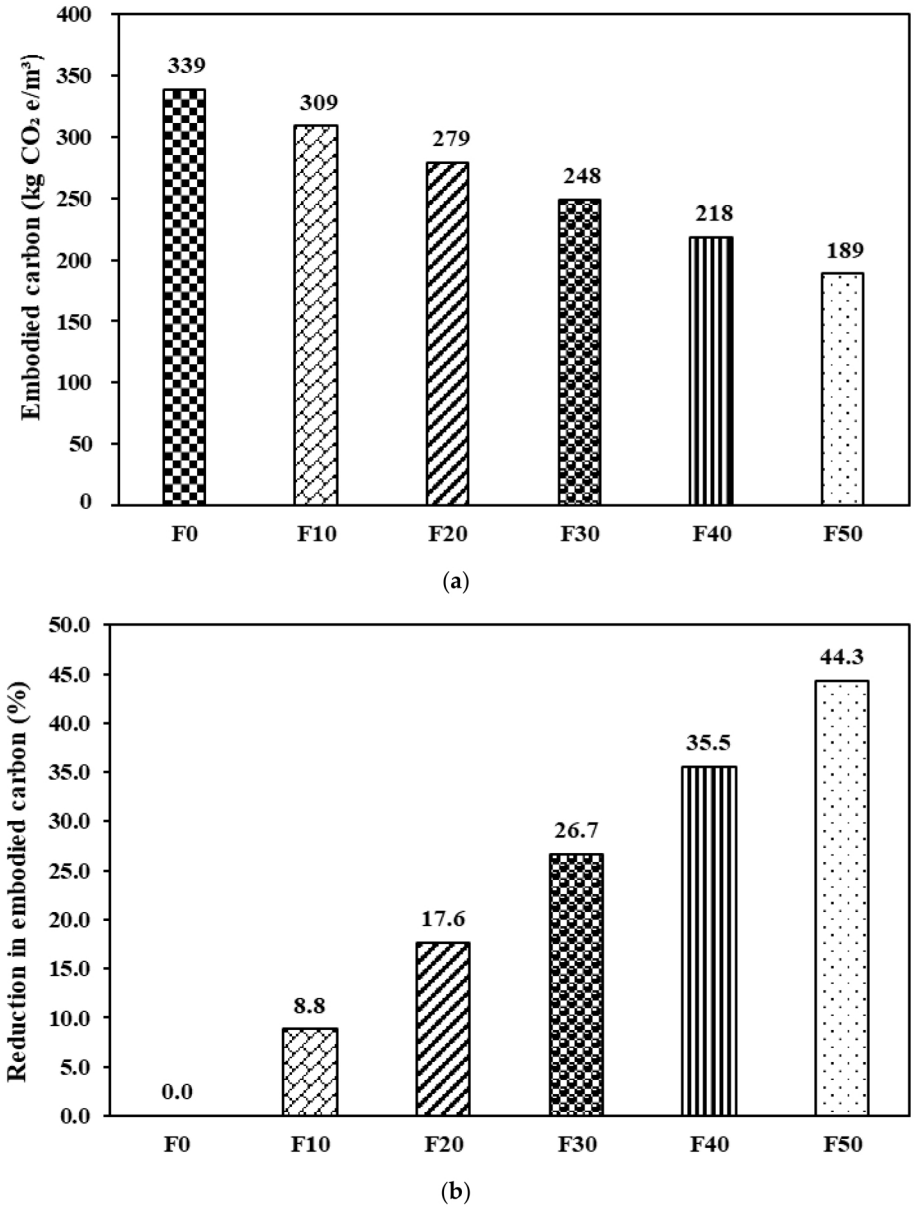


Figure 9. (**a**) Embodied carbon of slag cement mortars; (**b**) slag cement mortar reduction in embodied carbon.

As a supplementary performance-normalized indicator, the embodied carbon per unit of 28-day compressive strength was calculated by dividing the embodied carbon per cubic meter by the corresponding 28-day compressive strength. The resulting values were 11.81, 10.25, 12.89, 13.80, 13.83, and 16.73 kg $CO_2e \cdot m^{-3} \cdot MPa^{-1}$ for F0, F10, F20, F30, F40, and F50, respectively. F10, therefore, exhibited the lowest strength-normalized carbon intensity. Moreover, only F0 and F10 satisfied the plant-specific early-age production criteria. Consequently, the nominal 44% carbon reduction obtained for F50 should not be interpreted as a functionally equivalent reduction for the intended rapid-demolding application.

However, the absolute values depend on the generic emission factors, the assumed transport distance, and the adopted slag proxy. They also exclude curing energy, carbonation uptake, allocation alternatives, and end-of-life scenarios. The results should therefore be used to compare the investigated formulations under consistent assumptions and not as complete life-cycle carbon footprints.

5. ANOVA-Based Assessment of Slag Replacement Level Impact on Mortar Mechanical Properties

To determine whether the amount of slag significantly affected the mechanical performance of the mortars, the 28-day compressive and flexural strength results were analyzed using one-way analysis of variance (ANOVA) at a significance level of 0.05. The analysis was based on the replicate test results obtained for each formulation. The null hypothesis assumed that the average strength did not differ among the mortar mixtures, whereas the alternative hypothesis indicated that at least one formulation exhibited a different mean value. Whenever the ANOVA result was significant ($p < 0.05$), Tukey's honestly significant difference (HSD) test was applied to identify which mixtures differed from one another. Prior to conducting the one-way ANOVA, the normality of the residuals was assessed using the Shapiro–Wilk test, whereas the homogeneity of variances among groups was verified using Levene's test. For compressive strength, both assumptions were satisfied (Shapiro–Wilk $p = 0.943$; Levene's test $p = 0.719$). For flexural strength, the homogeneity of variances was confirmed (Levene's test $p = 0.217$), while the Shapiro–Wilk test indicated a slight deviation from normality ($p = 0.035$). Given the equal sample size across all groups and the robustness of ANOVA to minor departures from normality, the analysis was considered appropriate for the present data. This statistical evaluation was used to determine the slag replacement range within which the mortar could retain acceptable mechanical performance and to identify the replacement levels associated with a marked reduction in strength.

The ANOVA results shown in Table 3 confirm that slag replacement significantly affects the compressive strength. The calculated p-value ($p = 5.75 \times 10^{-14}$) is far below the significance level ($\alpha = 0.05$), indicating a statistically significant effect of slag replacement on compressive strength. This could be linked to the changes in hydration mechanisms as well as the densification of the matrix.

Table 3. ANOVA p-values for compressive and flexural strengths.

Property	Compressive Strength	Flexural Strength
p-value	5.75×10^{-14}	9.36×10^{-17}

Similarly, the ANOVA results indicate that slag content also has a statistically significant effect on flexural strength. The calculated p-value ($p = 9.36 \times 10^{-17}$) is significantly lower than 0.05, confirming that flexural behavior is also strongly correlated with the slag replacement percentage.

Table 4 shows the groups for each mixture according to Tukey's HSD post hoc test. When analyzing compressive strength, F0 and F10 are included in Group A, which means they have similar results. This reinforces the observation that a low level of substitution does not affect the compressive strength of slag-incorporated mortars. F20, F30, F40, and F50 are included in Groups B, C, D, and E, respectively.

Considering flexural strength, F10, F0, F20, F30, F40, and F50 are classified into Groups A, B, C, D, E, and F, respectively, indicating that each formulation exhibits statistically significant differences from other mixes, which demonstrates that slag replacement has a pronounced effect on the flexure performance of the mortars.

Additionally, the mean values of both compressive and flexural strengths reveal that strength decreases with the slag replacement level, indicating a systematic influence of slag content on mechanical performance.

Table 4. Tukey HSD groupings for compressive and flexural strengths.

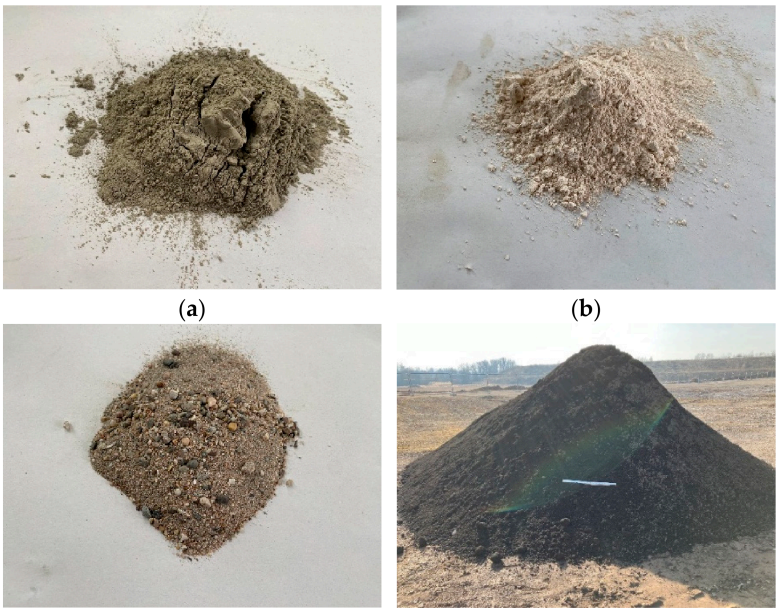
Mortar Mixture	Mean	Grouping: Compressive Strength	Mortar Mixture	Mean	Grouping: Flexural Strength
F10	30.16	A	F10	6.79	A
F0	28.71	A	F0	6.2	B
F20	21.64	B	F20	5.77	C
F30	17.97	C	F30	4.79	D
F40	15.76	D	F40	3.96	E
F50	11.3	E	F50	2.92	F

6. Materials and Methods

6.1. Materials

6.1.1. Cement

The cement used was Portland cement classified as CEM II/A-LL 52.5 R (Figure 10a), in accordance with the NF EN 197-1 standard [61]. It has an apparent density of 3100 kg/m^3, a specific area of 5373 cm^2/g, and an initial setting time of 45 min. Its compressive strength reaches 30 MPa at 2 d and 52.5 MPa at 28 d. Selected chemical properties of the CEM II/A-LL 52.5 R cement, as reported in the available supplier documentation, are presented in Table 5.



(**a**) (**b**) (**c**) (**d**)

Figure 10. (**a**) Portland cement CEM II/A-LL 52.5 R; (**b**) BETOCARB® HP-MX limestone filler; (**c**) natural sand 0–4 mm; and (**d**) parent 0–8 mm slag.

Table 5. Selected chemical properties of CEM II/A-LL 52.5 R cement.

Chemical Composition	SO_3	MgO	Na_2O	Cl^-
Weight (%)	<4	0.29	<0.1	<0.1

6.1.2. BETOCARB® HP-MX Limestone Filler

The limestone filler used in this study, presented in Figure 10b, is the commercial product BETOCARB® HP-MX, supplied by Omya and produced in Maxey, France. It

served as a mineral to improve the packing density and workability of the mortar. It has a density of 2700 kg/m^3 with 85% and 70% of the particles passing the 0.125 mm and 0.063 mm sieves, respectively. The filler exhibits a specific surface area of 7000 cm^2/g, and an activity index of 0.8. The chemical and physical properties, as provided in the supplier's technical data sheet, are reported in Table 6.

Table 6. Chemical and physical properties of BETOCARB® HP-MX limestone filler.

Property	Value	Unit
Chemical Properties		
Calcium carbonate, $CaCO_3$	98.0	%
Total carbonates	98.7	%
Chloride	0.0006	%
Sulfates	0.02	%
Total sulfur	0.06	%
Total organic carbon	0.06	%
SiO_2	0.1	%
Na_2O equivalent	0.001	%
Methylene blue value	0.4	g/kg
Physical Properties		
Particles passing 2 mm	100	%
Particles passing 0.125 mm	91	%
Particles passing 0.063 mm	79	%
Blaine specific surface area	720	m^2/kg
Activity index	0.85	—
Moisture content	0.2	%
Particle density	2.7	g/cm^3
Tapped bulk density	1.4	g/cm^3

The reported properties were obtained from the supplier's technical data sheet. No independent XRD analysis, complete particle-size distribution measurement, or SEM-based particle morphology characterization was performed.

6.1.3. Sand

The sand used in this investigation has a particle-size range of 0/4 mm (Figure 10c), complying with the specifications outlined in NF EN 12620 [62]. It has a density of 2590 kg/m^3, a water absorption of 1.1%, and a sand equivalent value of 81.3. Prior to mixing, the sand was air-dried to control the water content in the mix design.

6.1.4. Admixture

Premia 595 from CHRYSO was used as a superplasticizer to enhance the workability of the mixes. The admixture dosage was fixed at 0.5% of the binder mass and kept constant for all mixtures.

6.1.5. Blast Furnace Slag

The blast furnace slag used in this study was obtained from TEERAG-ASDAG and supplied as an industrial material with an initial particle-size range of 0–8 mm (Figure 10d). The parent material was characterized before sieving, while only the fraction passing 64 µm was incorporated into the mortar mixtures. The parent slag and the particle-size-classified fraction are therefore described separately below.

Parent 0–8 mm Slag

The parent slag was supplied with a nominal particle-size range of 0–8 mm. Before particle-size classification, the material was analyzed by an ISO/IEC 17025 [63] accredited laboratory. The characterization included moisture content, loss on ignition, total organic carbon, hydrocarbons, polycyclic aromatic hydrocarbons, volatile organic compounds, polychlorinated biphenyls, total trace element contents, and batch leaching according to EN 12457-4 [64].

The parent 0–8 mm material had a moisture content of 19.9%, a loss on ignition of 12.88% at 550 °C, and a total organic carbon content of 6.12%. The C10–C40 hydrocarbon content was 80 mg/kg dry matter, while the sum of the measured polycyclic aromatic hydrocarbons was 12.6 mg/kg dry matter. Benzene, toluene, ethylbenzene, xylenes, polychlorinated biphenyls, and the investigated chlorinated solvents were below their respective analytical quantification limits.

Selected total trace element concentrations are reported in Table 7. The highest measured concentrations were those of Zn and Pb, reaching 6310 and 903 mg/kg dry matter, respectively. These values represent total concentrations in the solid material and do not directly indicate the fraction that may be released under environmental exposure.

Table 7. Heavy metals and trace elements in parent slag.

Element	Content (mg/kg MS)
Zn	6310
Pb	903
Cr	122
Ni	88
Cu	28
Cd	<QL
Hg	<QL

QL: Quantification limit.

A batch-leaching test was conducted on the parent 0–8 mm material according to NF EN 12457-4 [64]. The eluate exhibited a pH of 8.8 and an electrical conductivity of 175 µS/cm. Selected leachate concentrations are presented in Table 8. These results provide an initial indication of the release behavior of the parent slag under the applied batch-leaching conditions.

Table 8. Leaching test results for the parent 0–8 mm slag before sieving.

Parameter	Value
pH	8.8
Electrical conductivity	175 µS/cm
As	0.0122 mg/L
Cd	<0.0001 mg/L
Cr	0.0012 mg/L
Cu	0.0018 mg/L
Hg	<0.0001 mg/L
Ni	0.0011 mg/L
Pb	0.0302 mg/L
Zn	0.144 mg/L
Chloride	0.1 mg/L
Sulfate	6.1 mg/L
Fluoride	4.9 mg/L
Dissolved solids	105 mg/L

Although the parent slag contained measurable total concentrations of trace elements, including Zn and Pb, total solid concentrations do not directly represent their environmental mobility. The NF EN 12457-4 batch-leaching test showed substantially lower concentrations in the aqueous eluate, including 0.144 mg/L Zn and 0.0302 mg/L Pb. Cementitious matrices may further reduce trace element mobility through physical encapsulation, precipitation, sorption onto hydration products, and chemical incorporation into hydrated phases [65]. However, these mechanisms were not directly evaluated in the present study because leaching tests were not performed on the hardened mortars. Consequently, the available results provide an initial characterization of the parent 0–8 mm slag but do not constitute a complete assessment of the long-term environmental behavior or regulatory compliance of the MP-BFS mortars.

However, the recovered MP-BFS fraction was not further characterized by X-ray diffraction (XRD), scanning electron microscopy (SEM), complete particle-size distribution analysis, or amorphous content quantification. Consequently, the mineralogical composition, particle morphology, and proportion of reactive amorphous phases were not directly determined in this study and represent limitations when interpreting the hydraulic reactivity and performance of MP-BFS.

The environmental analyses were performed on the parent 0–8 mm slag before sieving and not directly on the fraction passing 64 µm or on the hardened mortar specimens. Furthermore, the results do not constitute a complete regulatory assessment for construction product reuse because the applicable acceptance criteria depend on the intended application and national regulatory framework. Long-term immobilization and release of trace elements from the hardened cementitious matrices were not assessed in the present study.

Minimally Processed Blast Furnace Slag

The parent 0–8 mm slag was subjected only to particle-size classification by sieving, and the fraction passing 64 µm was recovered for incorporation into the mortar mixtures. No additional grinding, granulation, thermal treatment, mechanical activation, or chemical activation was applied. This fraction is therefore referred to throughout the manuscript as minimally processed blast furnace slag (MP-BFS).

6.2. Mix Design

The mortar mixtures were designed in accordance with the requirements of NF EN 196-1 [66]. Mortar mixtures were formulated with MP-BFS replacement levels of 0%, 10%, 20%, 30%, 40%, and 50% by mass of cement, corresponding to formulations F0, F10, F20, F30, F40, and F50, respectively. For all mixtures, the binder-to-sand (b/s) ratio was maintained constant at 1/3, while a polycarboxylate-based superplasticizer was added at a fixed dosage of 0.5% of the binder mass. The mixing water content was adjusted for each formulation to obtain the same workability in the fresh state, resulting in slump/spread values ranging between 23 and 24 cm, as illustrated in Figure 11. This choice reflects the industrial formulation procedure, in which the fresh mortar must satisfy a prescribed rheological performance to ensure casting, compaction, surface finishing, and production reproducibility rather than the water-to-powder ratio. This formulation strategy improves the industrial relevance of the comparison but introduces water demand as an additional variable. Consequently, the effects observed at high MP-BFS replacement levels cannot be attributed exclusively to slag incorporation. The increased water-accessible porosity, water uptake, and reduction in strength may result from the combined effects of Portland cement dilution, limited early-age MP-BFS reaction, increased water content, and changes in particle packing.

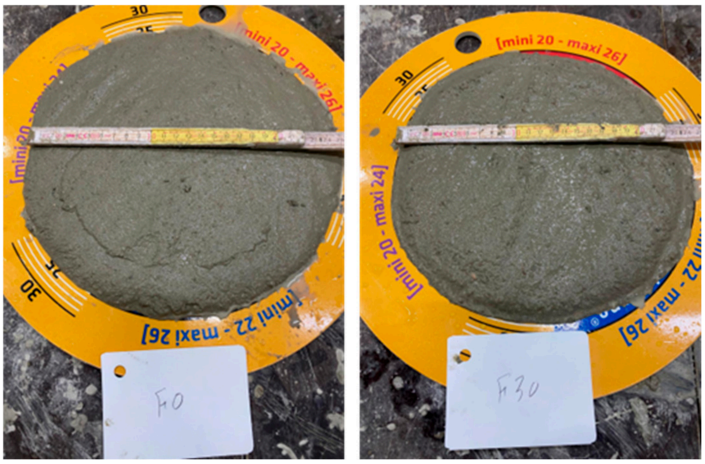


Figure 11. Flow test for F0 and F30.

The mix proportions of all mortar formulations are presented in Table 9. Mixing was performed using a mechanical mixer. Initially, cement, MP-BFS, limestone filler, and sand were blended for 60 s at low speed to ensure homogeneity. The fresh mortars were cast into molds in two layers. Prismatic specimens with dimensions of 40 × 40 × 160 mm were prepared for physical, mechanical, and water absorption tests (Figure 12), while cubic specimens measuring 100 × 100 × 100 mm were cast for capillary absorption measurements. Each layer was compacted using a vibrating table to eliminate entrapped air and ensure uniform compaction. After pouring, the surfaces of the test specimens were leveled using a metal trowel. Immediately after casting, the molds were covered with plastic film to limit moisture loss and were placed in a climate-controlled chamber maintained at 40 ± 2 °C and 50% relative humidity. At 8 h, the specimens were demolded. The specimens assigned to the 8 h mechanical tests were tested immediately after demolding, whereas the remaining specimens were returned to the same curing chamber and maintained at 40 ± 2 °C and 50% relative humidity until 24 h. At 24 h, the specimens assigned to the 24 h mechanical tests were tested, while the specimens intended for later-age testing were transferred to the factory ambient conditions of 20 °C and 50% relative humidity and stored under these conditions until their scheduled testing ages.

Table 9. Mix proportions (kg/m^3).

Formulation	F0	F10	F20	F30	F40	F50
Cement	392	353	314	274	235	196
Limestone filler	47	47	47	47	47	47
MP-BFS	0	39	78	118	157	196
Sand	1328	1328	1328	1328	1328	1328
Admixture	2.352	2.352	2.352	2.352	2.352	2.352
Water	185	190	195	200	205	215
Nominal w/b *	0.42	0.43	0.44	0.45	0.47	0.49

* b = Cement + limestone filler + MP-BFS.

This curing procedure was selected to reproduce the targeted industrial production cycle. In the plant, demolding takes place approximately 8 h after casting, whereas handling and transfer of the elements take place after approximately 24 h. The initial temperature of 40 °C therefore represents the actual elevated-temperature curing conditions used during the early production stage rather than conventional standard laboratory curing. No parallel standard-cured series was included because the objective was to compare the formulations under the actual plant-specific production cycle. Therefore, the absolute results should not be extrapolated directly to conventional standard curing conditions.



Figure 12. Mortar samples.

In this study, the binder was defined as the combined mass of cement, limestone filler, and MP-BFS. Accordingly, the w/b ratio increased from 0.42 for F0 to 0.49 for F50. Since the hydraulic contribution of MP-BFS was not independently quantified, these ratios should not be interpreted as equivalent effective reactive water-to-binder ratios. The increasing water demand is therefore considered together with cement dilution and MP-BFS characteristics when interpreting the results.

6.3. Experimental Program

Unless otherwise stated, all experimental results reported in this study correspond to mean values calculated from replicate specimens. The number of replicates used for each experimental test is specified in the corresponding sections. Standard deviations are reported in tables where available, while figures present the mean values for clarity.

6.3.1. Physical Properties: Water-Accessible Open Porosity and Bulk Density

Water-accessible open porosity and bulk density of the mortars were determined using a water-displacement method based on hydrostatic weighing, in accordance with NF P 18-459 [67] (Figure 13). All experimental operations, except for drying, were carried out at a controlled temperature of (20 ± 2) °C. The test specimens were soaked under vacuum to ensure optimal pore saturation. The samples were placed in a container connected to a vacuum device and then subjected to a pressure of 25 mbar or less for at least (4 ± 0.5) h. Water was then gradually introduced into the container while maintaining the reduced pressure for (44 ± 1) h. Mass characteristics were determined successively in the immersed state, in the soaked state with a dry surface, and in the dry state. After saturation, the test specimens were weighed fully immersed in water using a hydrostatic balance. The samples were then removed, carefully wiped to remove surface water without extracting the water contained in the pores, and immediately weighed in air. Finally, the test specimens were dried at (105 ± 5) °C until a constant mass was reached. The combination of dry mass, saturated mass, and immersed mass measurements enabled the determination of both water-accessible open porosity, corresponding to the volume of interconnected open pores, and bulk density of the mortar specimens, using the standardized relationships specified in NF P 18-459 [67]. Three specimens per formulation were tested for water-accessible open porosity and bulk density, and the reported values correspond to the average of these replicates.

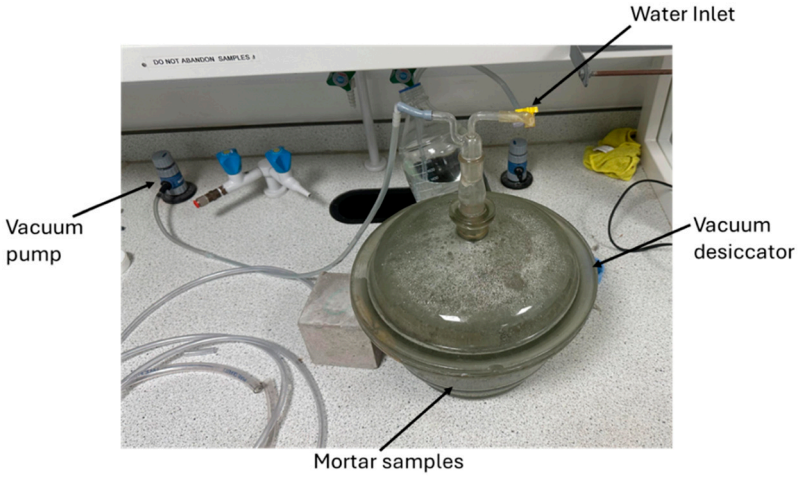


Figure 13. Water-accessible open porosity test.

6.3.2. Physical Properties: Water Absorption

Total Water Absorption

The determination of the total water absorption capacity of the mortars was carried out according to NF P18-459 [67]. After oven-drying at 28 d, the specimens were cooled down to room temperature and immersed in water. Specimens were removed from the water after 48 h, dried on the surface with a cloth, and then weighed. Total water absorption was determined based on the relative mass variation between the oven-dried and saturated states, expressed as a percentage of the dry mass. Three specimens of each mix were tested, and the value reported was the average of the replicates.

Capillary Water Uptake

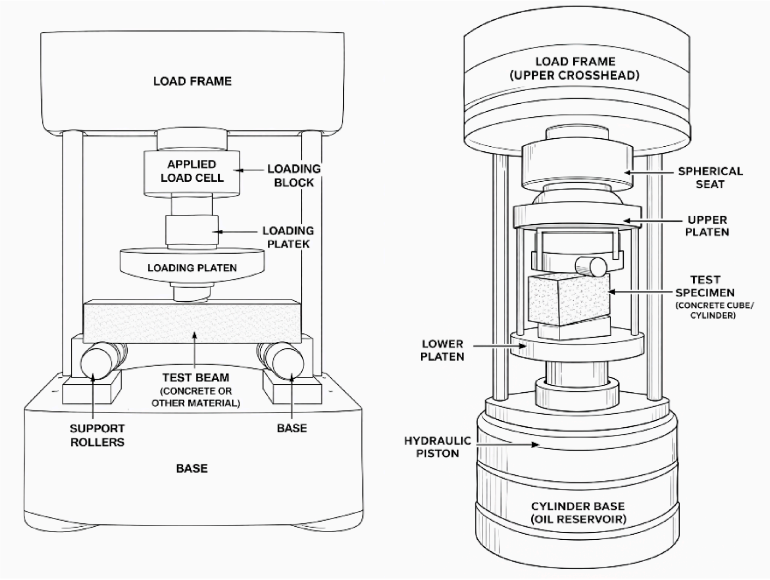
Capillary water uptake was determined at 28 d according to ASTM C1585 [68]. Three specimens for each mortar mix were oven-dried at 80 °C until constant mass and cooled to room temperature. The lateral sides were sealed with a non-absorbent coating, leaving only the exposed face in contact with water. The samples were then placed in a container filled with water up to 5 mm from the bottom of the samples. Mass variations due to water absorption were measured at time intervals of 3, 5, 10, 20, 30, 60, 120, and 240 min and at 24, 48, and 72 h.

6.3.3. Mechanical Properties: Flexural and Compressive Strengths

Flexural strength was determined in accordance with NF EN 196-1 [66] using a three-point bending configuration. Mortar prisms measuring 40 × 40 × 160 mm were examined at ages of 8 h, 1 d, 7 d, 28 d, and 90 d. Until testing, the specimens were maintained under the controlled conditioning regime described previously. The bending tests were carried out using a 250 kN electromechanical testing machine (IGM) fitted with a 50 kN load cell, with the load applied continuously at a rate of 50 N/s, as specified in NF EN 196-1 [66] (Figure 14a). At each testing age, three prisms were examined for every formulation, and the average flexural strength was reported.

Following the flexural test, the two fractured halves obtained from each prism were used for the determination of compressive strength at the same testing ages. Compression tests were carried out using the same testing machine, fitted with a 250 kN load cell, with the load applied at a constant rate of 2.4 kN/s in accordance with NF EN 196-1 [66] (Figure 14b). The compressive strength was calculated by dividing the maximum load sustained at failure by the loaded cross-sectional area of the specimen. Since three prisms were initially tested in flexure for each formulation and age, six half-prism specimens

were available for compression testing. Accordingly, the reported compressive strength represents the average value obtained from six test results.



(**a**) (**b**)

Figure 14. (**a**) Flexural strength equipment; (**b**) compressive strength equipment.

6.4. Industrial Early-Age Acceptance Criteria

The selection of the 8 h and 24 h testing ages was based on the organization of the industrial production line, which operates in three consecutive 8 h shifts. The 8 h age represents the intended demolding stage at the end of one shift, while the 24 h age represents the subsequent lifting and handling stage.

For the investigated production process, a mixture was considered suitable for demolding when its mean compressive strength at 8 h was at least 8 MPa. It was considered suitable for handling at 24 h when its mean compressive strength was at least 12 MPa. The 24 h criterion is not sufficient by itself to authorize lifting because the final handling requirement also depends on the structural verification of the precast element and on the design, location, embedment, and capacity of the lifting anchors or inserts.

These thresholds are plant-specific operational criteria applied to the compressive strengths measured on mortar half-prisms according to NF EN 196-1. They are not presented as direct equivalents of the cube or cylinder strengths used in structural lifting standards.

7. Conclusions

The objective of this study was to assess the potential for replacing cement with minimally processed blast furnace slag obtained by sieving an industrial 0–8 mm material below 64 µm, without grinding, additional granulation, thermal treatment, or chemical activation, as part of an industrial mortar production process. Unlike most studies based on ground, mechanically activated, or chemically activated blast furnace slag, the principal novelty of this work lies in the direct incorporation of a minimally processed industrial slag fraction, thereby limiting additional energy-intensive processing. The formulations were based on an imposed workability target (23–24 cm) and were discussed from an industrial production viewpoint, considering the plant-specific requirements of 8 MPa at 8 h for demolding and 12 MPa at 24 h before handling. The findings detailed below are the result of experimental work supported by empirical modelling efforts and environmental assessment of different slag-incorporating formulations.

- Mechanical performance

Flexural and compressive strengths were shown to be particularly sensitive to slag addition at early ages. While the compressive strength of the control mortar (0% slag) was only slightly surpassed by the mortar containing 10% slag (reaching 8.32 MPa at 8 h and 14.56 MPa after 1 day), increasing slag content led to a pronounced drop in early-age strength. After 8 h of hydration, compressive strengths of 6.95 MPa, 4.33 MPa, 2.99 MPa, and 1.64 MPa were recorded for slag contents of 20%, 30%, 40%, and 50%, respectively. After 28 days of hydration, replacement with slag between 30% and 50% led to mortar strengths that were only 63% to 39% of the reference strength, highlighting a dilution effect at both early and standard curing ages.

- Later-age strength evolution

Strength gain between 28 and 90 days showed that all MP-BFS mortars continued to develop strength, which is consistent with a possible delayed contribution of MP-BFS together with continued cement hydration. Unfortunately, this delayed strength gain was not able to compensate for the early strength drop observed when replacing cement with more than 20% slag. After 90 days of hydration, compressive strengths were 15% to 57% lower than that of the control for slag contents between 20% and 50%, respectively. However, these mechanisms remain hypotheses based on the observed macroscopic behavior and require confirmation through direct microstructural and hydration characterization.

- Porosity and water-related properties

Water-accessible open porosity decreased from 8.95% for F0 to 8.01% for F10 and subsequently increased with the replacement level, reaching 24.45% for F50. This water-accessible porosity was also accompanied by lower bulk densities and higher total and capillary water absorption values. F10 exhibited lower water-accessible open porosity and water uptake than the control, whereas higher MP-BFS contents exhibited increased water-accessible open porosity and water transport, suggesting a potentially more connected water-accessible pore network. Pore size distribution and pore connectivity were not measured directly.

- Link between porosity, transport, and strength

The empirical polynomial fit showed a strong association between MP-BFS content and water-accessible open porosity within the six investigated formulations (R^2 = 0.96). This evolution of porosity with slag content was directly related to increased water transport properties and decreased mechanical performance, suggesting that water-accessible open porosity is an important parameter influencing water transport and mechanical performance within the investigated mortar systems. However, the observed behavior was also influenced by cement dilution, increasing water demand, MP-BFS reactivity, and other unmeasured microstructural characteristics. The empirical regression equations developed in this study are therefore intended only to describe trends within the investigated experimental domain (0–50% MP-BFS replacement) and should not be extrapolated to other replacement levels, materials, or curing conditions without further validation.

- Environmental impact

Embodied carbon values of the studied mortars decreased quasi-linearly with slag content. A replacement level of 50% led to a reduction of ~44% compared to the reference mortar. Under the adopted system boundary and ICE emission factors, the reduction in embodied carbon was associated with the decrease in Portland cement content but also with the very low inherent carbon impact of MP-BFS. The reported carbon reductions should therefore be interpreted as comparative estimates rather than complete life-cycle results, as

curing energy, carbonation, alternative slag-allocation approaches, and end-of-life scenarios were excluded.

- Practical implications

Under the plant-specific screening criteria, F10 was the only MP-BFS-containing formulation that satisfied both the 8 h demolding requirement of 8 MPa and the 24 h handling requirement of 12 MPa. F20–F50 did not satisfy the 8 h demolding criterion and are therefore not suitable for the investigated rapid-demolding production cycle without further reformulation or process optimization. Accordingly, 10% MP-BFS represents the most suitable replacement level for the intended application under the investigated conditions. Higher replacement levels provide larger nominal embodied carbon reductions but are not functionally equivalent for this rapid industrial production scenario.

The study did not directly evaluate pore size distribution, hydration products, particle packing, or hardened mortar microstructure. In addition, water transport measurements should not be interpreted as direct evidence of long-term durability, since carbonation, chloride ingress, sulfate attack, freeze–thaw resistance, and alkali–silica reaction were not investigated. Future work should therefore combine microstructural and hydration analyses with long-term durability testing and plant-specific environmental data. In particular, characterization of hydration products, amorphous phase content, pore size distribution, and particle morphology of the recovered MP-BFS fraction would be required to validate the mechanisms proposed in this study, including delayed hydration, particle packing effects, and pore network evolution.

Author Contributions: Conceptualization, H.A. and H.G.; methodology, H.A. and H.G.; formal analysis, H.A. and H.G., investigation, H.A., L.F., G.A.-M., F.A., A.Y. and H.G.; writing—original draft preparation, H.A., G.A.-M. and H.G.; writing—review and editing, H.A., L.F., G.A.-M., F.A. and A.Y.; validation, L.F., G.A.-M. and F.A.; project administration, L.F. All authors have read and agreed to the published version of the manuscript.

Funding: This research received no external funding.

Data Availability Statement: Data generated and analyzed in this study are presented within the manuscript. Further inquiries can be directed to the corresponding authors.

Acknowledgments: The authors thank the FEHR Group Laboratory for the facilities and assistance provided during the experimental work.

Conflicts of Interest: Houssam Affan and Laurent Fehr were employed by Groupe FEHR. All authors declare no conflicts of interest.

References

1. Scrivener, K.L.; John, V.M.; Gartner, E.M. Eco-efficient cements: Potential economically viable solutions for a low-CO_2 cement-based materials industry. *Cem. Concr. Res.* **2018**, *114*, 2–26. [CrossRef]
2. Chen, S.; Teng, Y.; Zhang, Y.; Leung, C.K.Y.; Pan, W. Reducing embodied carbon in concrete materials: A state-of-the-art review. *Resour. Conserv. Recycl.* **2023**, *188*, 106653. [CrossRef]
3. Provis, J.L. Alkali-activated materials. *Cem. Concr. Res.* **2018**, *114*, 40–48. [CrossRef]
4. Xu, L.; Sun, Z.; Chen, Y.; Yang, K.; Yang, X.; Wu, K.; Lothenbach, B. Retardation mechanism of zinc on Portland cement and alite hydration. *Cem. Concr. Res.* **2024**, *184*, 107571. [CrossRef]
5. Ohemeng, E.A.; Ramabodu, M.S.; Nena, T.D.; Ohemeng, E.A.; Ramabodu, M.S.; Nena, T.D. Utilization of Blast Furnace Slag as an Enhancer in Masonry Mortars Made with Thermally Treated Waste Concrete Powder. *Buildings* **2023**, *13*, 2616. [CrossRef]
6. Bae, S.-H.; Lee, J.-I.; Choi, S.-J. Characteristics of Mortars with Blast Furnace Slag Powder and Mixed Fine Aggregates Containing Ferronickel-Slag Aggregate. *Materials* **2021**, *14*, 5879. [CrossRef] [PubMed]
7. Hallet, V.; De Belie, N.; Pontikes, Y. The impact of slag fineness on the reactivity of blended cements with high-volume non-ferrous metallurgy slag. *Constr. Build. Mater.* **2020**, *257*, 119400. [CrossRef]

8. Jura, J. Analysis of the Impact of Sludge and Slag Waste on the Basic Properties of Cement Mortars. In *System Safety: Human–Technical Facility–Environment*; Paradigm, Quality and Production Managers Association: Częstochowa, Poland, 2023; pp. 130–141. [CrossRef]
9. Kumar, P.; Gogineni, A.; Ammarullah, M.I. Sustainable bioengineering approach to industrial waste management: LD slag as a cementitious material. *Discov. Sustain.* **2025**, *6*, 242. [CrossRef]
10. Mohammed, S.H.; Fawzi, N.M. The Effect of the Utilization of Sustainable Materials on Some Mechanical Properties of Geopolymer Mortar, Engineering. *Technol. Appl. Sci. Res.* **2024**, *14*, 12464–12469. [CrossRef]
11. Shubbar, A.A.; Al-Jumeily, D.; Aljaaf, A.J.; Alyafei, M.; Sadique, M.; Mustafina, J. Investigating the Mechanical and Durability Performance of Cement Mortar Incorporated Modified Fly Ash and Ground Granulated Blast Furnace Slag as Cement Replacement Materials. In Proceedings of the 2019 12th International Conference on Developments in eSystems Engineering (DeSE), Kazan, Russia, 7–10 October 2019; pp. 434–439. [CrossRef]
12. Thakur, A. Enhancement in Properties of Cement Mortar by using Iron based Material—Critical Review. *Int. J. Res. Appl. Sci. Eng. Technol.* **2019**, *7*, 689–691. [CrossRef]
13. Santamaria, A.; Ortega-Lopez, V.; Skaf, M.; García, V.; Gaitero, J.J.; San-Jose, J.T.; González, J.J.; Santamaria, A.; Ortega-Lopez, V.; Skaf, M.; et al. Ladle furnace slag as cement replacement in mortar mixes. In Proceedings of the Sustainable Construction Materials and Technologies, London, UK, 14–17 July 2019. Available online: https://ekoizpen-zientifikoa.ehu.eus/documentos/5db974442999520a73d4181f?lang=en (accessed on 24 June 2026).
14. Zhang, L.-N.; Kwon, S.-J.; Wang, X.-Y. Low-Carbon Slag Concrete Design Optimization Method Considering the Coupled Effects of Formwork Stripping, Strength Progress, and Carbonation Durability. *Buildings* **2025**, *15*, 1316. [CrossRef]
15. Pal, S.C.; Mukherjee, A.; Pathak, S.R. Investigation of hydraulic activity of ground granulated blast furnace slag in concrete. *Cem. Concr. Res.* **2003**, *33*, 1481–1486. [CrossRef]
16. Juenger, M.; Provis, J.L.; Elsen, J.; Matthes, W.; Hooton, R.D.; Duchesne, J.; Courard, L.; He, H.; Michel, F.; Snellings, R.; et al. Supplementary Cementitious Materials for Concrete: Characterization Needs. *MRS Online Proc. Libr.* **2012**, *1488*, 8–22. [CrossRef]
17. Shi, C.; Roy, D.; Krivenko, P. *Alkali-Activated Cements and Concretes*; CRC Press: London, UK, 2003. [CrossRef]
18. Jacquemot, F. Accélération du Durcissement des Liants à Base de Laitier de Haut Fourneau pour les Produits Préfabriqués en Béton. Ph.D. Thesis, University of Lille 1, Villeneuve-d'Ascq, France, 2014. Available online: https://theses.fr/2014LIL10123 (accessed on 24 June 2026).
19. Li, L.; Ye, T.; Li, Y.; Wang, Z.; Feng, Z.; Liu, Z. Improvement of microporous structure and impermeability of cement mortars using fly ash and blast furnace slag under low curing pressures. *Constr. Build. Mater.* **2023**, *401*, 132890. [CrossRef]
20. Juenger, M.C.G.; Siddique, R. Recent advances in understanding the role of supplementary cementitious materials in concrete. *Cem. Concr. Res.* **2015**, *78*, 71–80. [CrossRef]
21. Subpa-asa, P.; Nito, N.; Fujiwara, S.; Date, S. Evaluation of the Prediction and Durability on the Chloride Penetration in Cementitious Materials with Blast Furnace Slag as Cement Addition. *Constr. Mater.* **2022**, *2*, 53–69. [CrossRef]
22. Wang, H.-Y.; Wang, W.-C.; Wang, J.C.; Chen, Y.-W. Evaluation of the engineering properties and durability of mortar produced using ground granulated blast-furnace slag and stainless steel reduced slag. *Constr. Build. Mater.* **2021**, *280*, 122498. [CrossRef]
23. Chen, H.-J.; Huang, S.-S.; Tang, C.-W.; Malek, M.A.; Ean, L.-W. Effect of curing environments on strength, porosity and chloride ingress resistance of blast furnace slag cement concretes: A construction site study. *Constr. Build. Mater.* **2012**, *35*, 1063–1070. [CrossRef]
24. Ghasemalizadeh, S.; Mehairi, A.G.; Zhao, D.; Khoshnazar, R. Combination of ultrafine granulated blast furnace slag and metakaolin in low portland cement clinker cementitious mixtures. *Mater. Struct.* **2025**, *58*, 285. [CrossRef]
25. Hall, C.; Hoff, W.D. *Water Transport in Brick, Stone and Concrete*, 3rd ed.; CRC Press: London, UK, 2021. [CrossRef]
26. Sadok, R.H.; Belas, N.; Tahlaiti, M.; Mazouzi, R. Reusing calcined sediments from Chorfa II dam as partial replacement of cement for sustainable mortar production. *J. Build. Eng.* **2021**, *40*, 102273. [CrossRef]
27. Yang, C.C.; Cho, S.W.; Wang, L.C. The relationship between pore structure and chloride diffusivity from ponding test in cement-based materials. *Mater. Chem. Phys.* **2006**, *100*, 203–210. [CrossRef]
28. Global Cement and Concrete Association (GCCA). *The GCCA 2050 Cement and Concrete Industry Roadmap for Net Zero Concrete*; Global Cement and Concrete Association: London, UK, 2021. Available online: https://gccassociation.org/concretefuture/ (accessed on 24 June 2026).
29. Buildings Department. *Code of Practice for Precast Concrete Construction 2003*; Government of the Hong Kong Special Administrative Region: Hong Kong, China, 2003. Available online: https://www.bd.gov.hk/doc/en/resources/codes-and-references/code-and-design-manuals/OldVersions/CoP_CPPCC_ov.zip (accessed on 24 June 2026).
30. *FD CEN/TR 15728*; Design and Use of Inserts for Lifting and Handling of Precast Concrete Elements. Afnor EDITIONS: La Plaine Saint-Denis, France, 2017. Available online: https://www.boutique.afnor.org/en-gb/standard/fd-cen-tr-15728/design-and-use-of-inserts-for-lifting-and-handling-of-precast-concrete-elem/fa149792/32153 (accessed on 24 June 2026).

31. Shi, C.; Jiménez, A.F.; Palomo, A. New cements for the 21st century: The pursuit of an alternative to Portland cement. *Cem. Concr. Res.* **2011**, *41*, 750–763. [CrossRef]
32. Hamdouni, S.; Benaicha, M.; Alaoui, A. Optimizing self-compacting concrete: Formulation approach enhanced by entropy method. *Discov. Civ. Eng.* **2024**, *1*, 63. [CrossRef]
33. Melais, F.Z.; Achoura, D.; Ghorbel, E. Durability of mortars containing blast furnace slags used as a partial substitute of Portland cement exposed to external sulfate attacks. *J. Mater. Environ. Sci.* **2021**, *12*, 837–852.
34. Edeb, B.; Allout, N.; Benkhelil, M.; Guettala, S. Optimizing High-Performance Concrete Properties Containing Blast Furnace Slag and Marble Powder. *Adv. Mater. Sci.* **2024**, *24*, 89–110. [CrossRef]
35. Tagba, M.; Li, S.; Jiang, M.; Gao, X.; Benmalek, M.L.; Boukour, S.; Liu, C. Performance Evaluation of Cementitious Composites Containing Granulated Rubber Wastes, Silica Fume, and Blast Furnace Slag. *Crystals* **2021**, *11*, 632. [CrossRef]
36. Ikhaddalene, S.; Irekti, A.; Oualit, M. Durability Indices of a Sealing Mortar Incorporating Blast Furnace Slag: Comparison with a Commercial Reference. *Period. Polytech. Civ. Eng.* **2025**, *69*, 1321–1332. [CrossRef]
37. Neville, A.M. *Properties of Concrete*; Pearson: Essex, UK, 2011.
38. Powers, T.C. Structure and Physical Properties of Hardened Portland Cement Paste. *J. Am. Ceram. Soc.* **1958**, *41*, 1–6. [CrossRef]
39. Affan, H.; Fehr, L.; Al-Massri, G.; Alassaad, F.; Yaghi, A.; Ghanem, H. Strength, Transport Properties, and Life Cycle Impacts of Mortar Containing German Natural Pozzolan. *Infrastructures* **2026**, *11*, 67. [CrossRef]
40. Al-Massri, G.; Ghanem, H.; Khatib, J.; El-Zahab, S.; Elkordi, A. The Effect of Adding Banana Fibers on the Physical and Mechanical Properties of Mortar for Paving Block Applications. *Ceramics* **2024**, *7*, 1533–1553. [CrossRef]
41. Papayianni, I.; Stefanidou, M. Strength–porosity relationships in lime–pozzolan mortars. *Constr. Build. Mater.* **2006**, *20*, 700–705. [CrossRef]
42. Sun, Y.; Wang, K.Q.; Lee, H.S. Prediction of compressive strength development for blended cement mortar considering fly ash fineness and replacement ratio. *Constr. Build. Mater.* **2021**, *271*, 121532. [CrossRef]
43. Benachour, Y.; Davy, C.A.; Skoczylas, F.; Houari, H. Effect of a high calcite filler addition upon microstructural, mechanical, shrinkage and transport properties of a mortar. *Cem. Concr. Res.* **2008**, *38*, 727–736. [CrossRef]
44. Li, Y.-X.; Chen, Y.-M.; Wei, J.-X.; He, X.-Y.; Zhang, H.-T.; Zhang, W.-S. A study on the relationship between porosity of the cement paste with mineral additives and compressive strength of mortar based on this paste. *Cem. Concr. Res.* **2006**, *36*, 1740–1743. [CrossRef]
45. Bentz, D.P.; Turpin, R. Potential applications of phase change materials in concrete technology. *Cem. Concr. Compos.* **2007**, *29*, 527–532. [CrossRef]
46. Scrivener, K.L.; Juilland, P.; Monteiro, P.J.M. Advances in understanding hydration of Portland cement. *Cem. Concr. Res.* **2015**, *78*, 38–56. [CrossRef]
47. Jennings, H.M. Refinements to colloid model of C-S-H in cement: CM-II. *Cem. Concr. Res.* **2008**, *38*, 275–289. [CrossRef]
48. Schiller, K.K. Strength of porous materials. *Cem. Concr. Res.* **1971**, *1*, 419–422. [CrossRef]
49. Mehta, P.K.; Monteiro, P.J.M. *Concrete: Microstructure, Properties, and Materials*, 4th ed.; McGraw-Hill Education: New York, NY, USA, 2014.
50. Salvini, V.; Pandolfelli, V.; Spinelli, D. Mechanical Properties of Porous Ceramics. In *Recent Advances in Porous Ceramics*; IntechOpen: London, UK, 2018. [CrossRef]
51. Papadakis, V.G. Effect of supplementary cementing materials on concrete resistance against carbonation and chloride ingress. *Cem. Concr. Res.* **2000**, *30*, 291–299. [CrossRef]
52. Circular Ecology. Concrete Embodied Carbon Footprint Calculator. Available online: https://circularecology.com/concrete-embodied-carbon-footprint-calculator.html (accessed on 24 June 2024).
53. *ISO 14044:2006*; Environmental Management—Life Cycle Assessment—Requirements and Guidelines. ISO: Geneva, Switzerland, 2006. Available online: https://www.iso.org/standard/38498.html (accessed on 11 October 2025).
54. Moazami, A.; Nabizadeh, M.; Komaei, A.; Soroush, A. Sustainable Soil Stabilization with Sodium Carbonate-Activated Slag, Pumice, Rice Husk, and Sugarcane Bagasse Ashes: A Life Cycle Assessment Approach. *Results Eng.* **2025**, *27*, 106900. [CrossRef]
55. Hartman, H.; Williams, J.J. *Materials: An Environmental Primer*; RIBA Publishing: London, UK, 2024.
56. Maroszek, M.; Rudziewicz, M.; Shah, S.M.A.; Tran, D.H.; Hebda, M.; Maroszek, M.; Rudziewicz, M.; Shah, S.M.A.; Tran, D.H.; Hebda, M. Development of Eco-Friendly Construction Materials for 3D Printing Using Fly Ash and Demolition Waste. *Buildings* **2025**, *15*, 3988. [CrossRef]
57. Ishaque, S. Life Cycle Analysis on the Extraction of $Ca(OH)_2$ from Industrial Waste Products for Use in a Passive-DAC System for CO_2 Capture. Master's Thesis, University of Gothenburg, Gothenburg, Sweden, 2025.
58. Durdziński, P.T.; Haha, M.B.; Bernal, S.A.; De Belie, N.; Gruyaert, E.; Lothenbach, B.; Méndez, E.M.; Provis, J.L.; Schöler, A.; Stabler, C.; et al. Outcomes of the RILEM round robin on degree of reaction of slag and fly ash in blended cements. *Mater. Struct./Mater. Constr.* **2017**, *50*, 135. [CrossRef]

59. Fisher, L.V.; Barron, A.R. The recycling and reuse of steelmaking slags—A review. *Resour. Conserv. Recycl.* **2019**, *146*, 244–255. [CrossRef]
60. Sourmelis, S.; Pontikes, Y.; Myers, R.J.; Tennant, M. Business models for symbiosis between the alumina and cement industries. *Resour. Conserv. Recycl.* **2024**, *205*, 107560. [CrossRef]
61. *NF EN 197-1*; Ciment—Partie 1: Composition, Spécifications et Critères de Conformité des Ciments Courants. Afnor EDITIONS: La Plaine Saint-Denis, France, 2012. Available online: https://www.boutique.afnor.org/fr-fr/norme/nf-en-1971/ciment-partie-1-composition-specifications-et-criteres-de-conformite-des-ci/fa149898/1234 (accessed on 24 June 2026).
62. *NF EN 12620+A1*; Granulats Pour Béton. Afnor EDITIONS: La Plaine Saint-Denis, France, 2008. Available online: https://www.boutique.afnor.org/fr-fr/norme/nf-en-12620-a1/granulats-pour-beton/fa157250/31276 (accessed on 25 December 2025).
63. Reference Standards. MedChemExpress. Available online: https://www.medchemexpress.com/standards.html (accessed on 24 June 2026).
64. *NF EN 12457-4*; Caractérisation des Déchets—Lixiviation—Essai de Conformité pour Lixiviation des Déchets Fragmentés et des Boues—Partie 4: Essai en Bâchée Unique avec un Rapport Liquide/Solide de 10 L/kg et une Granularité Inférieure à 10 mm (sans ou avec Réduction de la Granularité). Afnor EDITIONS: La Plaine Saint-Denis, France, 2002. Available online: https://www.boutique.afnor.org/fr-fr/norme/nf-en-124574/caracterisation-des-dechets-lixiviation-essai-de-conformite-pour-lixiviatio/fa104284/20762 (accessed on 24 June 2026).
65. Chen, Q.Y.; Tyrer, M.; Hills, C.D.; Yang, X.M.; Carey, P. Immobilisation of heavy metal in cement-based solidification/stabilisation: A review. *Waste Manag.* **2009**, *29*, 390–403. [CrossRef] [PubMed]
66. *NF EN 196-1*; Méthodes d'Essais des Ciments—Partie 1: Détermination des Résistances. Afnor EDITIONS: La Plaine Saint-Denis, France, 2016. Available online: https://www.boutique.afnor.org/fr-fr/norme/nf-en-1961/methodes-dessais-des-ciments-partie-1-determination-des-resistances/fa184622/57803 (accessed on 24 June 2026).
67. *NF P18-459*; Concrete—Testing Hardened Concrete—Testing Porosity and Density. Afnor EDITIONS: La Plaine Saint-Denis, France, 2022. Available online: https://www.boutique.afnor.org/en-gb/standard/nf-p18459/concrete-testing-hardened-concrete-testing-porosity-and-density/fa160729/34961 (accessed on 24 June 2026).
68. *ASTM C1585-20*; Standard Test Method for Measurement of Rate of Absorption of Water by Hydraulic-Cement Concretes. ASTM: West Conshohocken, PA, USA, 2020. Available online: https://store.astm.org/c1585-20.html (accessed on 24 June 2026).

Disclaimer/Publisher's Note: The statements, opinions and data contained in all publications are solely those of the individual author(s) and contributor(s) and not of MDPI and/or the editor(s). MDPI and/or the editor(s) disclaim responsibility for any injury to people or property resulting from any ideas, methods, instructions or products referred to in the content.